CONF-930352--14
BNL--48363
DE93 007272

STRUCTURAL ANALYSIS OF AN UNDERGROUND REINFORCED CONCRETE WASTE STORAGE TANK DUE TO OVER-PRESSURIZATION*

J. XU[1], K. BANDYOPADHYAY[1], S. SHTEYNGART[1] AND H. ECKERT[2]

ABSTRACT

This paper presents the results of a structural analysis performed by use of the finite element method in determining the pressure-carrying capacity of an underground tank which contains nuclear wastes. The tank and surrounding soil were modeled and analyzed using the ABAQUS program. Special emphases were given on determining the effects of soil-containment interaction by employing Coulomb friction model. The effect of material properties was investigated by considering two sets of stress-strain data for the steel plates. In addition, a refined mesh was used to evaluate the strain concentration effects at steel liner thickness discontinuities.

1.0 INTRODUCTION

The structural capacity of concrete containments to sustain internal pressure build-up and the attempts to gain knowledge of such structural behavior by numerical techniques have been subjects in the nuclear industry for many years. A good understanding of the structural behavior of concrete containments could substantially facilitate decision makings on issues in nuclear power plants relating to design, safety, as well as environmental concerns. Significant efforts have been made by the industry, researchers and government regulatory institutions to standardize the analysis approach. For instance, the Sandia 1:6 scale concrete containment experiment and the collective effort to pre- and post- predict the results by means of finite element methods (1-3) improved the analyses techniques for containments of light water reactors. There are, however, a different type of concrete containment structures used for storage of nuclear wastes that have not been investigated extensively. The waste storage tank structures are different from those encountered in nuclear power plants in that the waste storage tanks are underground structures. Recent designs of the high-level waste storage tanks basically consist of a primary steel tank enclosed by a steel-lined concrete containment. The structural integrity of such tanks is crucial for maintaining a clean environment and has become a major issue as a result of recent nuclear waste cleanup efforts. This paper deals with the structural

---

*This work was performed under the auspices of the U.S. Department of Energy.

[1]Brookhaven National Laboratory, Upton, New York 11973

[2]U.S. Department of Energy, Germantown, Maryland 20585-0002

response of a waste storage tank under accidental internal pressures and, especially, with the structural behaviors affected by the soil-containment interaction, and strain concentrations at locations where thickness of the steel liner changes.

The waste tank structure under consideration is shown in Figure 1 which consists of a primary steel tank enclosed by a steel-lined reinforced concrete containment, and contains semi-liquid form of wastes. The concrete containment freely sits on the concrete foundation and is surrounded by the soil. Since the reinforced concrete is a non-homogeneous material an analysis of the concrete containment structure especially in the nonlinear range, employing the ductility failure criteria, represents a challenging computational effort. In addition, the tank-soil interaction effects, the nature of which, in most cases, is uncertain, further complicate the computation. In this study, a 2-D axisymmetric finite element model was developed using the general purpose program ABAQUS (4), and an analysis was performed considering large displacements and large strains, as well as material nonlinearities in the solution algorithm.

2.0 DESCRIPTIONS OF FINITE ELEMENT MODELS AND SOLUTION PROCEDURES

2.1 2-D Axisymmetric global model

The 2-D axisymmetric model using ABAQUS code, as shown in Figure 2, was developed for the purpose of establishing the global response of the tank and investigating its sensitivity to the variation of certain modeling parameters and deterioration of the steel under large strains. With the aid of the ABAQUS program, the primary tank and secondary steel liner were modeled with axisymmetric shell elements (SAX1). The reinforced concrete containment and the basemat were modeled with concrete elements using the REBAR options. In modeling the concrete sections, the basemat and containment wall were simulated with two layers of concrete elements embedded with reinforcing bars (rebars) based on the smeared hyper-elastic theory with consideration of tension stiffening, shear retention and rebar/concrete interaction in both compression and tension. The soft refractory concrete layer sandwiched at the base between the primary tank and the secondary liner was modeled as an elastic slab. Since the refractory concrete layer was mostly confined until the primary tank wall and dome lifted up during the course of loading, the bending effect of the modeled elastic slab was relatively insignificant. When the internal pressure was increased to a level at which the concrete in the dome is completely cracked, and the steel liner and rebars were at locations stretched beyond the yield point, the transverse shear carrying capacity of the concrete in the dome began to play an important role in further resisting the pressure load. Therefore, the mesh in the dome concrete region was refined with four layers of concrete elements across the thickness to more accurately model the transverse shear behavior of the dome concrete.

Since there are no structural connections between the primary steel tank and the refractory concrete layer at the base, between the secondary liner and the concrete basemat, and between the foot of the concrete containment wall and the basemat, the respective interfaces were simulated using the slideline elements (ISL21A) in ABAQUS assuming zero tangential friction within the interfaces. The interface elements allow separation from the prescribed surfaces.

The soil was modeled in two parts: a) the soil cover on top of the tank, and b) the soil surrounding the tank. The soft cover of soils of about 7 feet is modeled with quadratic axisymmetric elements (CAX4) with material properties based on a shear wave velocity of 300 ft/sec. The effects of the surrounding soil are complex and not well defined. Therefore, for the purpose of investigating the interaction of the soil with the tank, the Coulomb friction model was employed to simulate the soil effects. This was accomplished with the aid of ITS interface elements available in ABAQUS. The ITS elements have the capabilities to simulate compression effects normal to the interface and Coulomb friction tangential to the interface. In this soil interface model, the static earth pressure was converted to equivalent initial displacements of the springs normal to the ITS interface. The stiffness values of these springs are generated from a closed-form solution of an equidimensional equation for a horizontal section of a cylinder surrounded by the half-space with an applied uniform pressure inside the cylinder, as shown in Figure 3. The tangential friction in the interface is controlled by the prescribed Coulomb friction coefficient which allows for sensitivity study of the effect of the surrounding soil on the structural response of the tank. Finally, the basemat of the tank structure was modeled with uniform elastic springs (Winkler soil foundation) with material properties based on a shear wave velocity of 1200 ft/sec.

2.2 Refined local models for evaluation of strain concentrations induced at liner thickness variations

The approach to generate the solution for strain concentrations induced by the geometric discontinuities in the primary steel tank adopts the recommendations by Dameron, et al, (2). Three steps are involved in the approach:

1) 2-D axisymmetric global static analysis,

2) local refined mesh static analyses for discontinuity locations of interest,

3) peak strain evaluations

Step 1 was performed with the ABAQUS model described in Section 2.1. The solution for displacement vs. pressure histories at all respective locations which can later be used as boundary conditions for step 2 analysis were saved on tape. The local strain concentrations due to liner thickness variations were then computed

in Step 2 using refined meshes that detail the geometries at these locations. The meshes extended out from the discontinuity sections to the points at which the global behavior can be observed. The boundaries of the refined mesh were then supplied with the displacement vs. pressure histories from Step 1. A finite element analysis of the refined mesh was then performed. Two types of liner thickness changes were identified for the primary tank which are shown in Figure 4. Type (a) consists of two plates of different thicknesses connecting together through a smooth transition on one side to minimize the strain concentration at the joint and is located in the baseplate near the corner. Type (b) discontinuity has two plates with different thicknesses joined together with a sharp change in thickness on one. Such a step-like variation of thickness creates an eccentricity which could induce significant bending effects. The type (b) discontinuity has been identified in the dome near the apex. Finite element models for the two types of thickness changes are shown in Figure 5 in which 2-D axisymmetric line shell elements of type SAX1 were employed and the finite element meshes were located coincident with the center of the liner cross sections. In the mesh where the rigid beam is introduced, the multipoint constraints (MPC's) user subroutine simulating a rigid beam for the 2-D axisymmetric analysis was utilized.

The local peak strains at the discontinuities are then evaluated using the proposed formula:

$$\epsilon_{local} = K\beta\epsilon_{global} \tag{1}$$

In the above relation, K represents the strain concentration effect and is defined as:

$$K = (\epsilon_{eff})_{local}/\epsilon_{global}$$
$$where, (\epsilon_{eff})_{local} = \int\left[\frac{2}{3}\{d\epsilon^P d\epsilon^P\}\right]^{1/2} \tag{2}$$

in the which $d\epsilon^p$ represents the peak plastic strains generated in Step 2. The K factor can be developed either from experimental data or from analytical solutions. Relevant to the thickness discontinuities concerned herein, the data generated in Step 2 were used for calculation of the K factor.

The β factor in Equation 1 represents the effect of stress biaxiality because the ductility-based criterion, which is used here, is significantly affected by the multiaxial nature of the stress state. The β factor or the ductility factor is defined as

$$\beta = 2^{(BF-1)}$$

$$where,\ BF = (\sigma_1 + \sigma_2)/(\sigma_1^2 - \sigma_1\sigma_2 + \sigma_2^2)^{1/2} \qquad (3)$$

BF in the above equation is the Davis biaxiality factor (Reference 2).

With the values of K and β for a given pressure load obtained for each of the discontinuity types discussed above, the corresponding peak strain can be computed by use of Equation 1. Case studies are performed to investigate the structural behavior of the tank and its sensitivity to soil parameters.

3.0 CASE STUDIES AND DISCUSSIONS

The structural behavior of the tank was investigated by subjecting it to an internal static uniform pressure in addition to dead weight, the surrounding soil pressure and the hydrostatic pressure on the inside of the primary tank from the liquid waste. The concrete in the dome region was completely cracked at an internal pressure of about 40 psig while the containment wall and the basemat remained uncracked. The pressure load was increased gradually to 65 psig. The response parameters used to characterize the structural behavior of the tank are strains in the primary tank and up-lift displacements of the concrete containment. In order to investigate the effects of the soil friction, mechanical properties of steel, and liner geometric discontinuities upon the response parameters of the tank structure, three case studies were conducted: a) the base case with a mean stress-strain relationship for the steel plates (Figure 6) and Coulomb friction coefficient of 0.57 for the surrounding soil; b) a reduction of the Coulomb friction coefficient by half to estimate the effect of soil friction and c) replacement of the steel strength in the base case by a lower bound value (Figure 6) to assess the impact of liner strength on the structural response. A concrete compressive strength (f'_c) of 4ksi was used for all three cases. The strain concentration effects induced by the thickness variations were studied for the base.

For clarity, the locations at which the strains and displacements are presented are indicated in Figure 7. The results for all case studies are discussed in details below.

3.1 The Base Case

The base case employs a mean stress-strain relationship for the primary tank and the secondary liner and Coulomb soil friction coefficient of 0.57 which corresponds to a friction angle of 30^0. The deformed shape of the structure as the pressure was increased to 65 psig is shown in Figure 8. Two important observations are: a) radial outward deflection (bulging) of the primary tank wall and b)

separation of concrete wall from basement. The concrete containment wall lifted up as a rigid body by the pressure through the dome of the primary tank. The magnitude of uplift of the containment is largely controlled by two factors: a) the friction effect of the surrounding soil which tends to hold down the containment in place, and b) the bending stiffness values of the base plate of the primary tank and the secondary liner near the knuckle regions.

The structural response of the tank in terms of strains and displacements for the entire pressure history at selected locations are shown in Figures 9 through 12. The bottom knuckle regions were the first to yield at about 38 psig. The highest meridional strain due primarily to bending is about 5% at 65 psig occurring at the bottom knuckle region of the secondary liner. It is attributed to the uplift of the containment. The highest hoop strain (3.8%) occurs near the mid-wall section of the primary tank. The vertical displacement at the knuckle region D4 is almost the same as that at the hunch region D2, indicating a rigid body-type vertical movement of the containment wall. However, the vertical displacement at the top of the tank D1 is about 25% higher than the hunch region D2, resulting from bending and stretching of the dome. At 65 psig, the maximum vertical displacement of the dome is about 23 inches and the maximum horizontal displacement of the mid-wall section of the primary tank is about 17 inches.

3.2 Effect of Soil Friction on the Structural Response of the Tank

The effect of soil friction was studied by reducing the Coulomb friction coefficient μ by half. The deviations of strains and displacements from the base case are then plotted for the selected locations and shown in Figures 13 through 16. In these Figures, the subscript MH stands for the mean steel strength with half soil friction and MF represents the mean steel strength full soil friction.

For the hoop strains, Figure 13 indicates almost no change at locations E1, E2, and E6, and moderate reduction of 10 - 20% elsewhere compared to the base case. For the meridional strains, Figure 14 shows a much pronounced increase of about 75% at location E6 which is the bottom knuckle region of the secondary liner, a moderate increase at the location E5 which is the bottom knuckle region of the primary tank, and almost no effects elsewhere. The surrounding soil interacts with the tank as the pressure increases, providing a passive shear force (Coulomb friction) on the outer surface of the containment wall to prevent the containment from any movement. These observations are also confirmed by the displacement plots shown in Figures 15 and 16 which indicate that the tank dome moves upward by about 30% more than the base case. A reduction of the soil friction decreases this vertical shear resistance force and, therefore, the pressure load causes further bending of the knuckle regions allowing a larger vertical movement of the dome. This reduces the hoop strain due to the biaxiality effect.

3.3 Effect of Variation of Strength of Steel Plates on the Structural Response of the Tank

The material specification (i.e. ASTM designation) of the steel plates used for construction of the primary tank and secondary liner are known. However, the actual strength of the steel plates used is not known. Therefore, a literature search was conducted to determine the mean value of the strength of this steel grade obtained from various test programs. This mean value was used for the two cases discussed above in Sections 3.1 and 3.2. In order to determine the effect of steel strength on the nonlinear structural response, a case study was performed considering the strength specified by the code (identified as "lower-bound" in Figure 6).

Figures 17 through 20 present the results in which the subscript LF represents a lower-bound strength with full soil friction effect. The results are expressed in terms of the deviations of the response parameters from the base case. Regarding the hoop strains, as observed in Figure 17, the use of the lower-bound steel properties allows an increase of the strain level by about 80-100% in the wall section of the primary tank at 55-65 psig and has almost no impact elsewhere in the structure for the pressure range considered in this study. The reduction of the steel strength has a smaller effect on the meridional strain as depicted in Figure 18; even reductions in the strain level are observed at some locations. These observations are also confirmed by the displacement plots shown in Figures 19 and 20. The effects of the material strength can be explained by the fact that, as the strength decreases, the material reaches plasticity sooner (i.e., at a lower pressure) at which point the tank loses its stiffness substantially, and since the tank is constrained by the surrounding soil friction in the longitudinal direction, the pressure load carried by the tank increases the strain levels in the hoop direction.

3.4 Effects of Strain Concentration Induced by Geometric Discontinuities

As discussed in Section 2.2, strain concentration effects for two types of geometric discontinuities were analyzed by considering the base case (See Section 3.1). The strain concentration factor, K, and the stress biaxiality factor, β, were computed and the local peak strains calculated by use of Equation 1. The resulting peak strains are plotted together with the global strains at the same location. The hoop and meridional strains for the type (b) discontinuity which is located in the dome of the primary tank are presented in Figures 21 and 22. The meridional strains for the type (a) discontinuity which occurs in the base plate of the primary tank are shown in Figure 23. Since the base plate rests on concrete, the type (a) discontinuity at this location has no effect on the hoop strains. In all these three figures, the ratio of the local peak strain to the corresponding global strain represents the combined effect due to strain concentration and stress biaxiality.

For the type (a) discontinuity, the local peak strain in the longitudinal direction is about twenty-two times higher than the corresponding global strain at 65 psig. However, the local peak strain is only 1.1% since the global strain is very small at this location.

For the type (b) discontinuity, the local peak strains in both the longitudinal and meridional directions are about ten times higher than the corresponding global strains. The resulting maximum local strain is about 5% in the meridional direction.

4.0 CONCLUSIONS

In this paper, the results of a comprehensive structural analysis of an underground waste storage tank subjected to internal static pressures are presented. The analysis was continued up to a pressure of 65 psig. Other loads such as the gravity load, earth pressure and hydrostatic pressure were considered. Parametric case studies were performed to determine the effects of the soil and material parameters on the structural behavior of the tank.

The following conclusions can be drawn upon review of the results presented above:

1) For the base case which was studied using the best estimate of material properties, at an internal pressure of 65 psig, the highest hoop strain is about 3.8% occurring at the mid-wall section of the primary tank while the highest meridional strain is about 5% occurring at the bottom knuckle region of the secondary liner. The concrete containment moves upward primarily due to bending and stretching of the knuckles of both the primary tank and secondary liner. The concrete wall separates from the basemat and moves upward as a rigid body. The dome concrete is completely cracked at this pressure.

2) The effect of soil friction simulated by the Coulomb model was investigated by reducing the friction coefficient by half. The results indicate that the meridional strain at the bottom knuckle region of the secondary liner was increased by about 75% while the strains at other locations were less affected.

3) The use of a lower bound material strength for the steel plates reduces the strains at the bottom knuckle of the secondary liner. It, however, increases the hoop strain near the mid-wall section of the primary tank by about 80-100%.

4) The effects of strain concentration and stress biaxiality at a liner thickness discontinuity in the dome produces a local strain as high as 5% in the meridional direction at an internal pressure of 65 psig.

ACKNOWLEDGEMENT

The study was performed under a contract with the U.S. Department of Energy, Environmental Restoration and Waste Management (DOE-EM). Their support and constructive suggestions during the course of the study are gratefully acknowledged.

DISCLAIMER

REFERENCES

1. Clause, D.B., "Round Robin Pretest Analysis of a 1:6 Scale Reinforced Concrete Containment Model Subject to Static Internal Pressurization", NUREG/CR-4913, May 1987.

2. Dameron, et al., "Criteria and Guidelines for Predicting Concrete Containment Leakage", EPRI Report NP-6260-M, 1989.

3. Costantino, C., et al., "NFAP Calculation of the Response of 1/6 Scale Reinforced Concrete Containment Model", the 10th SMiRT, Anaheim, California, 1989.

4. "ABAQUS User's Manual", Version 4.9.1, Hibbitt, Karlsson & Sorensen, Inc., Pawtucket, Rhode Island, 1991.

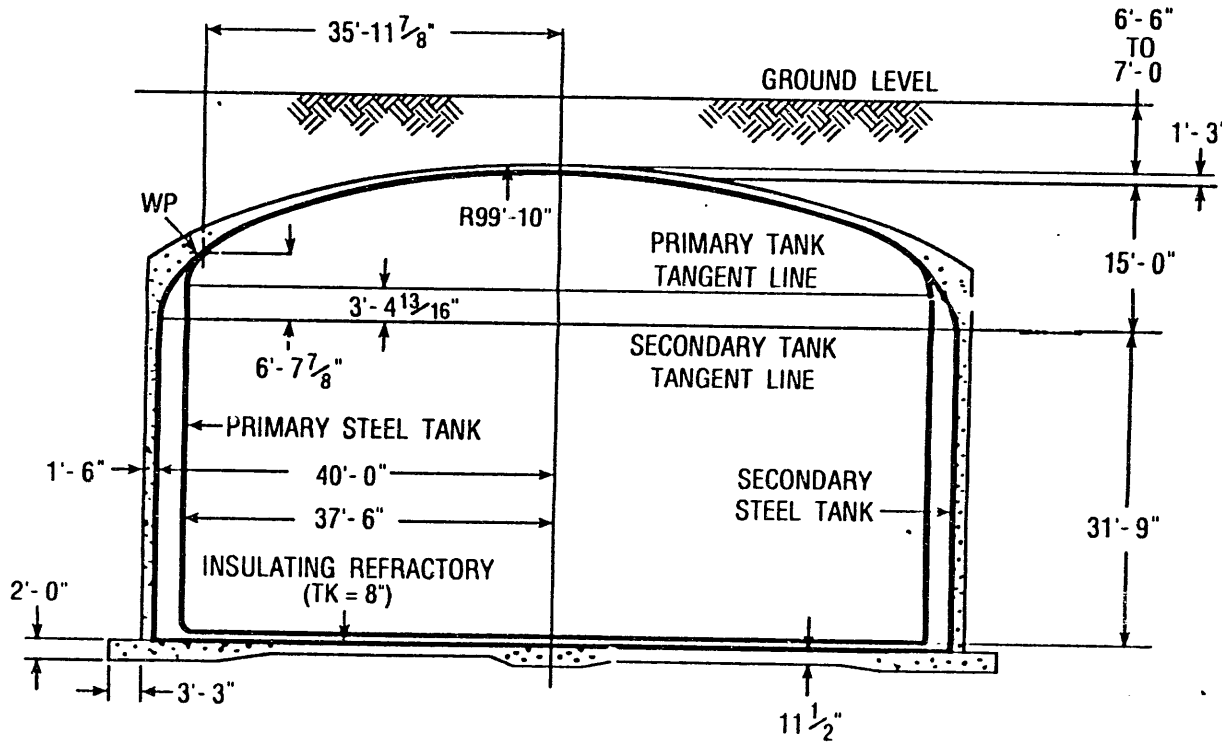

Figure 1 Double Shell Tank Diagram

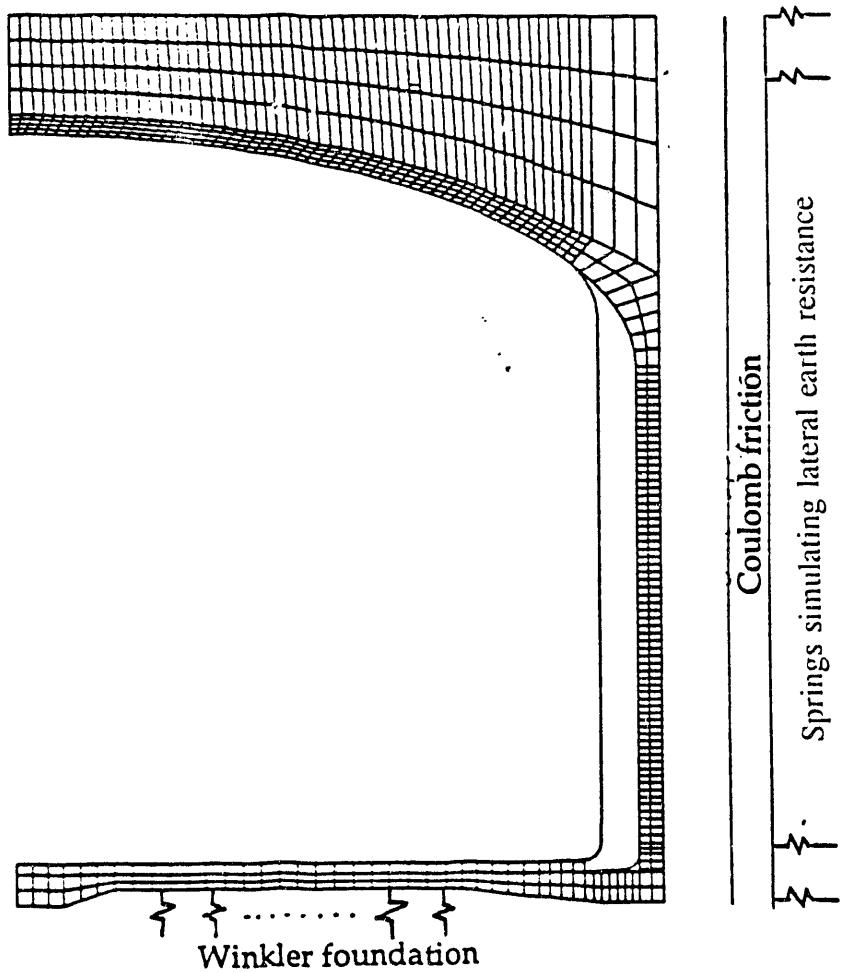

Figure 2 Finite Element Mesh Plot

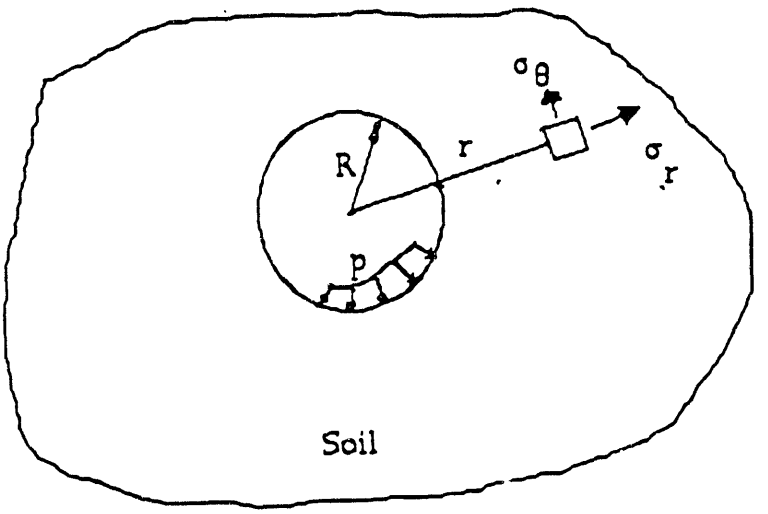

Figure 3 Plan View of a Horizontal Section of the Half Space for Generating Spring Stiffness Simulating Lateral Earth Resistance with a Cylindrical Opening

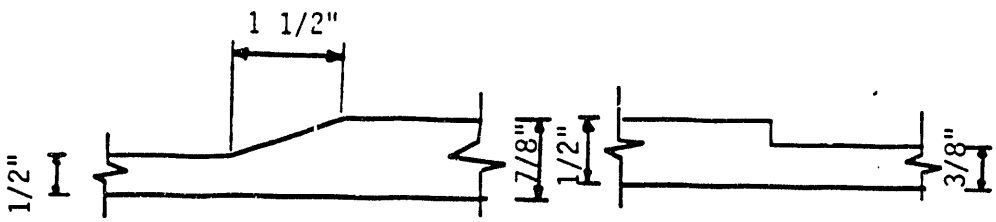

(a) (b)

Figure 4 Two Types of Liner Thickness Changes

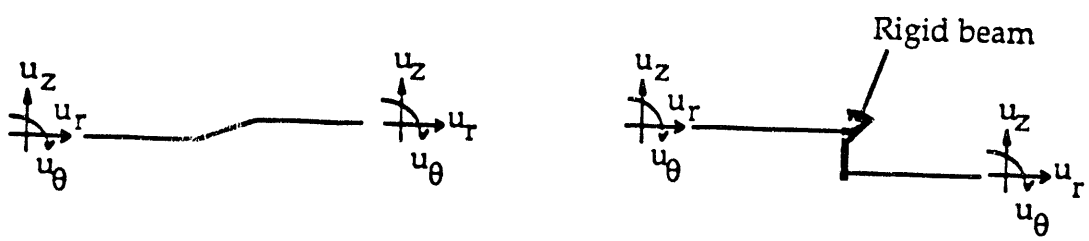

(a) (b)

Figure 5 Refined Finite Element Models for Liner Discontinuities

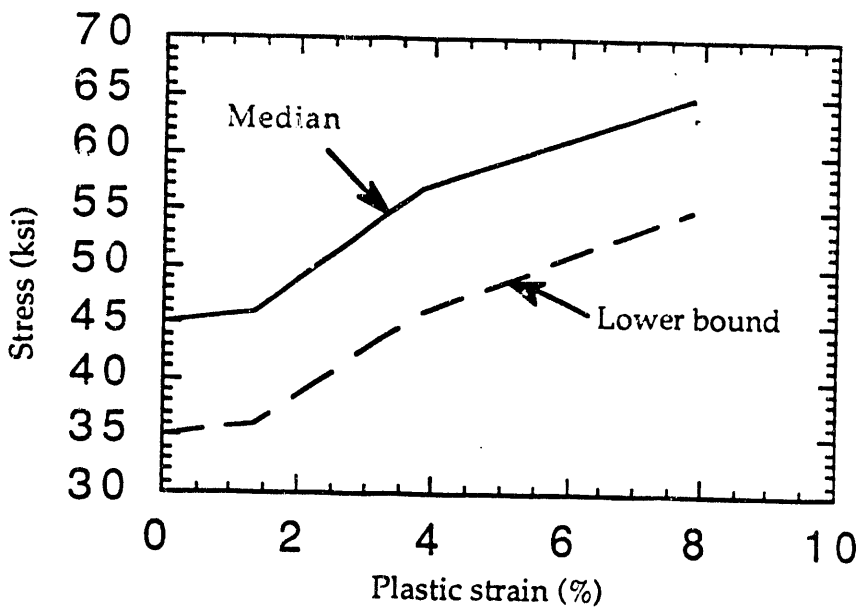

Figure 6 Stress-Plastic Strain Curve for Steel Plates

E ----- Strain output locations.
D ---- Displacement output locations.

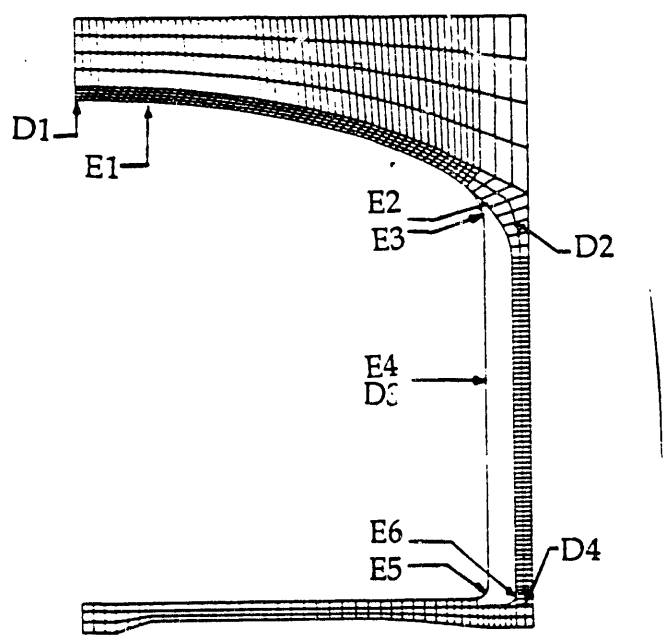

Figure 7. Strains and displacements output locations.

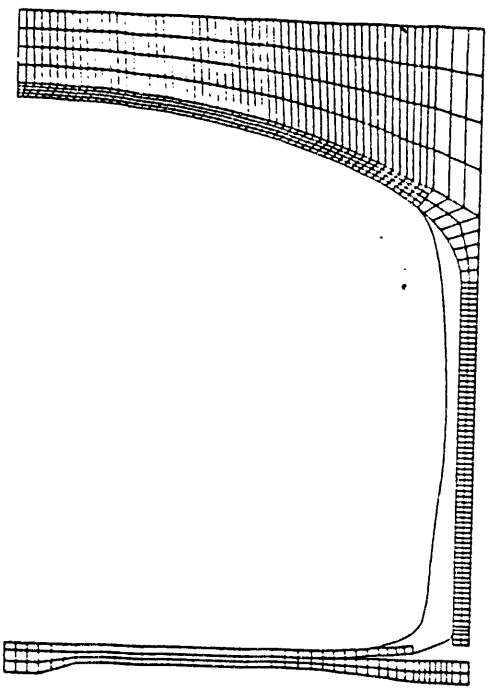

Figure 8 Deformed Shape of the Tank for the base case at 65 psig

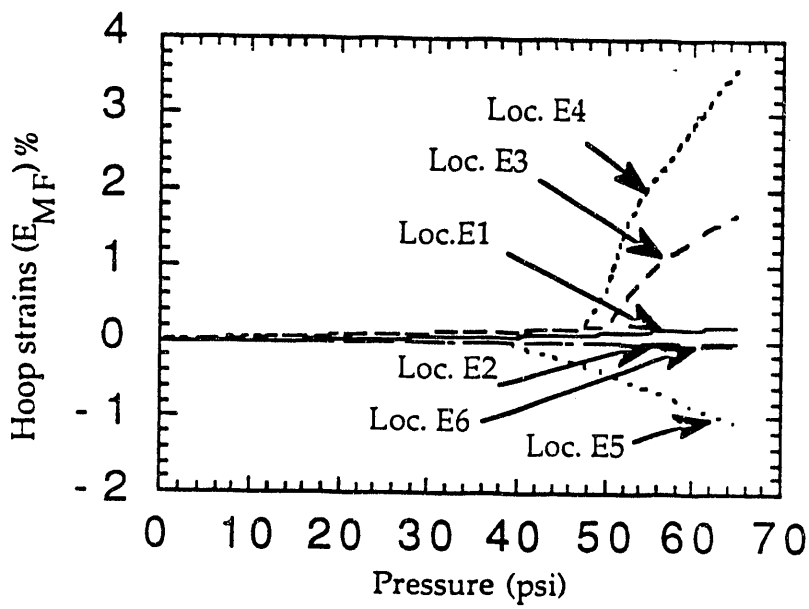

Figure 9 Hoop Strains with Mean Steel Strength and Full Friction Effect (base case)

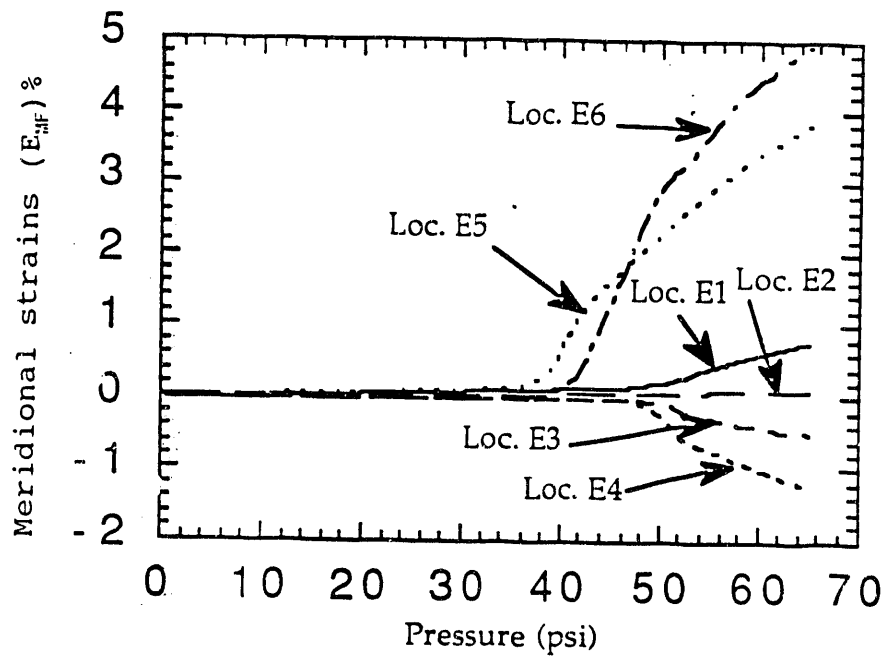

Figure 10 Meridional Strains with Mean Steel Strength and Full Friction Effect (base case)

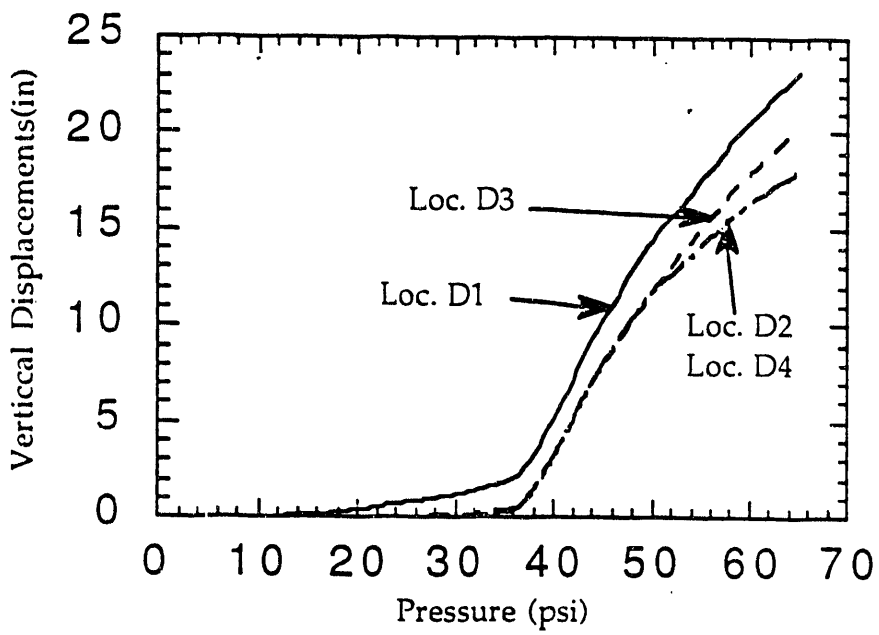

Figure 11 Vertical Displacements with Mean Steel Strength and Full Friction Effect (base case)

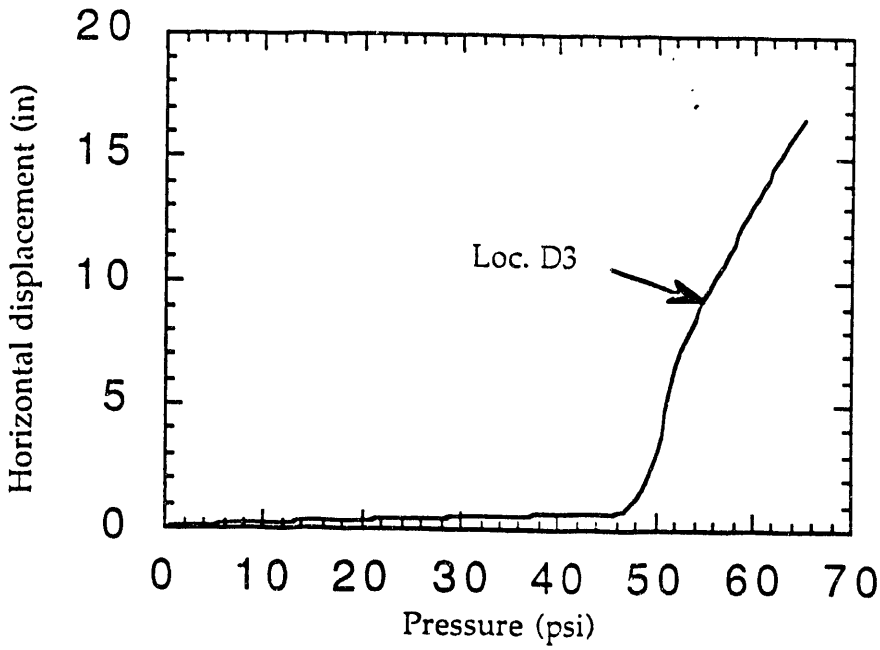

Figure 12 Horizontal Displacement with Mean Steel Strength and Full Friction Effect (base case)

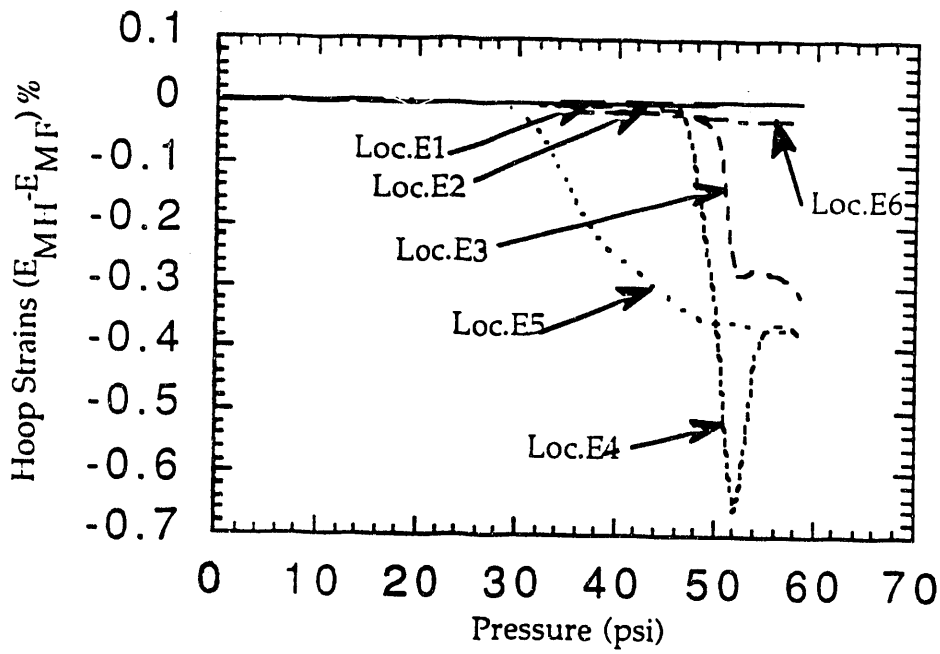

Figure 13. Soil friction effects on hoop strains.

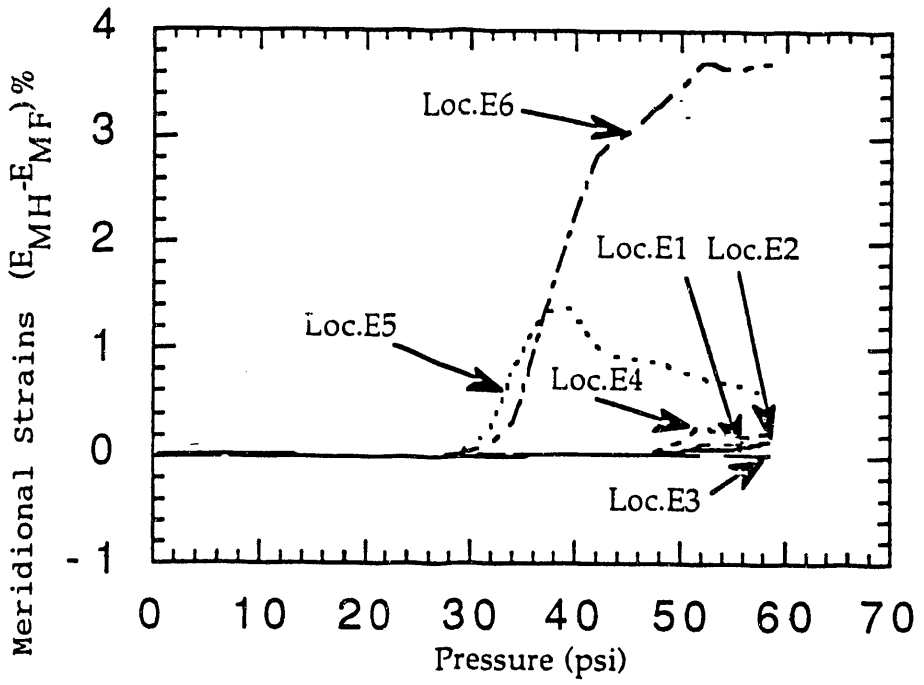

Figure 14 Soil friction effects on meridional strains

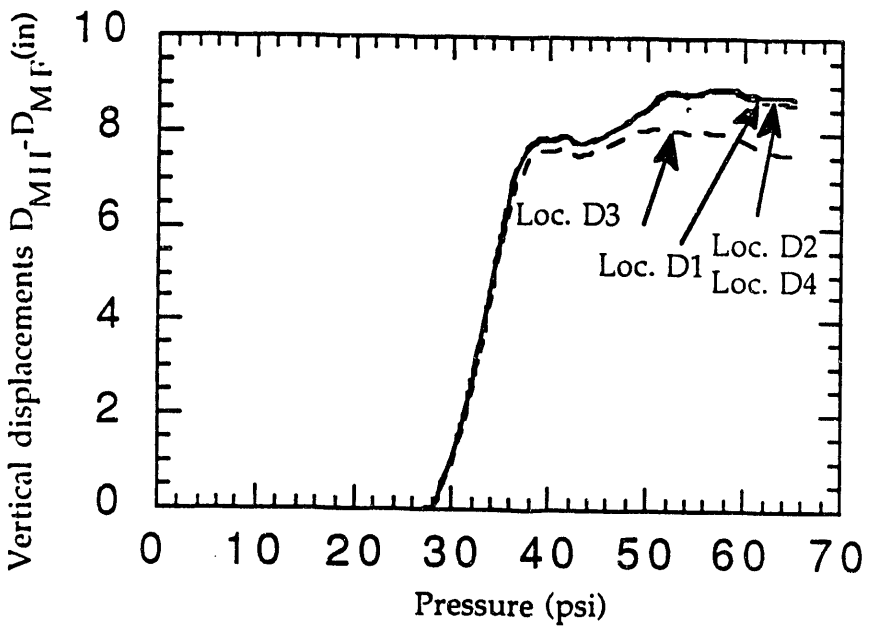

Figure 15. Soil friction effect on vertical displacements.

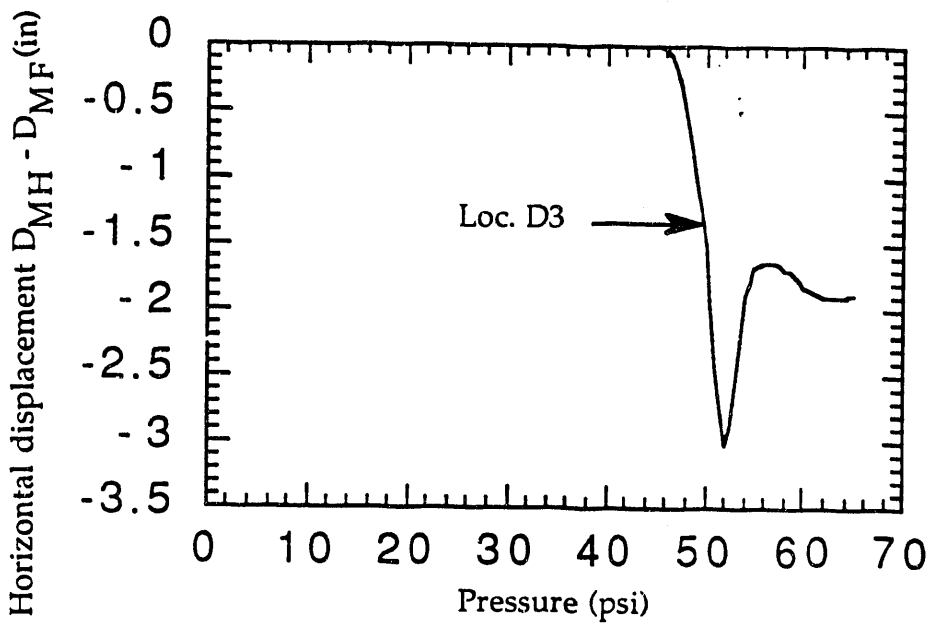

Figure 16. Soil friction effect on horizontal displacement

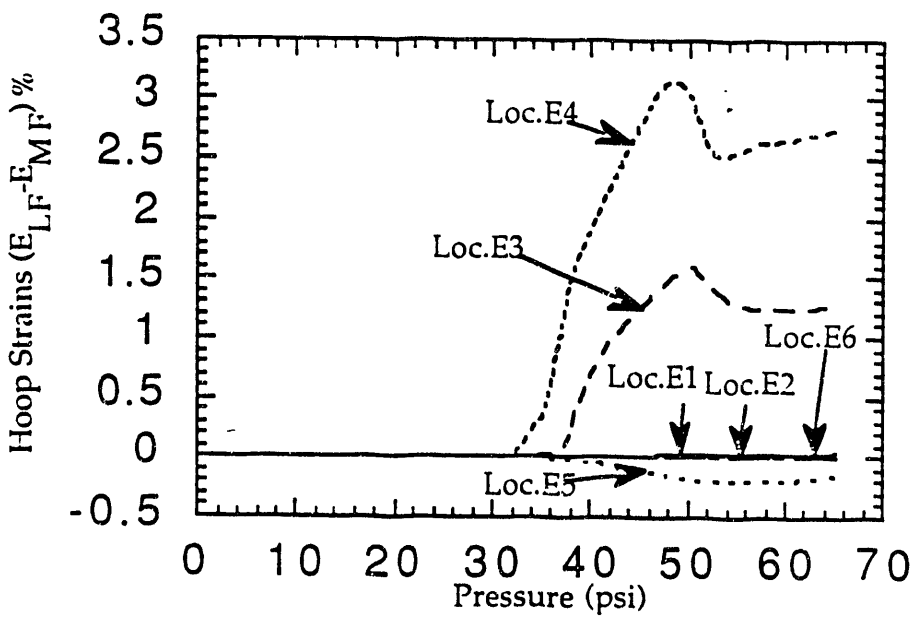

Figure 17 Effect of Steel Plate Strength on Hoop Strains

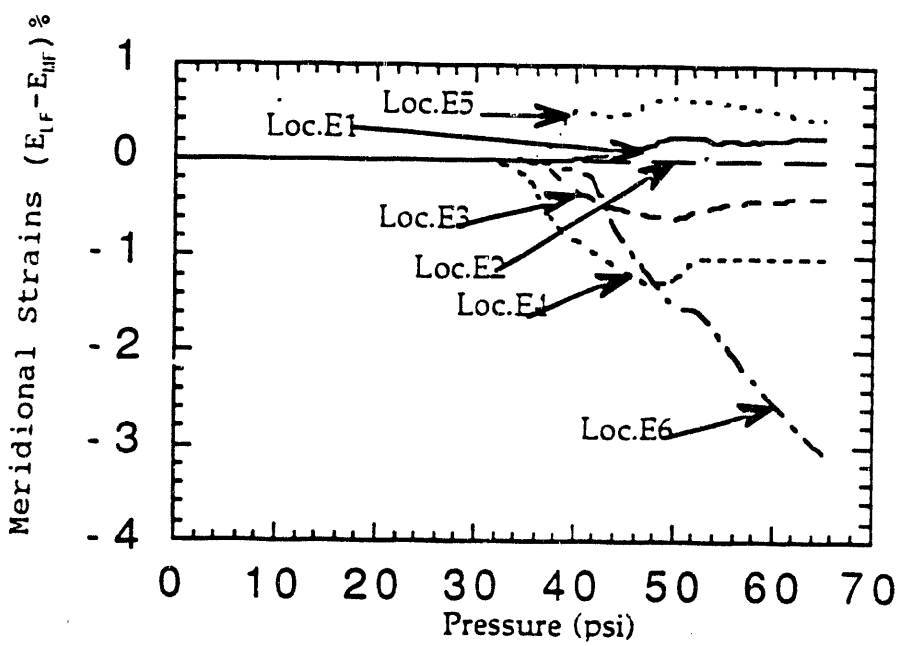

Figure 18 Effect of steel plate strength on meridional strains

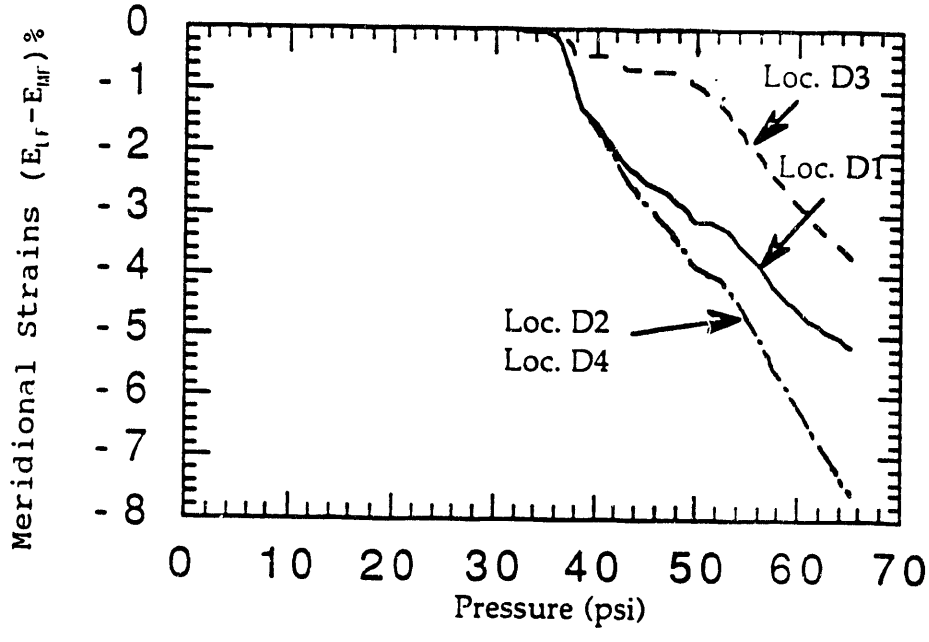

Figure 19 Effect of Steel Plate Strength on Vertical Displacements

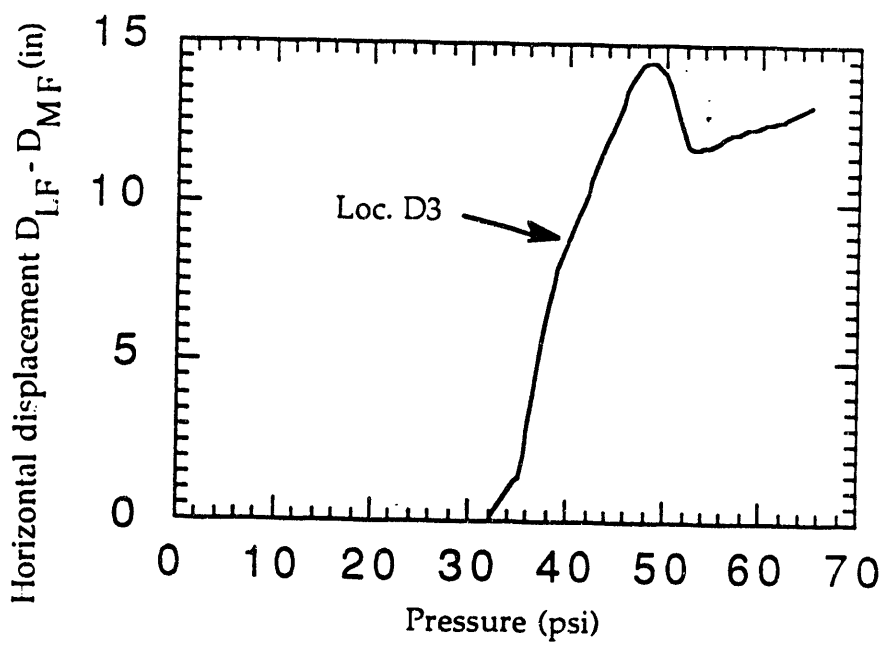

Figure 20 Effect of Steel Plate Strength on Horizontal Displacement

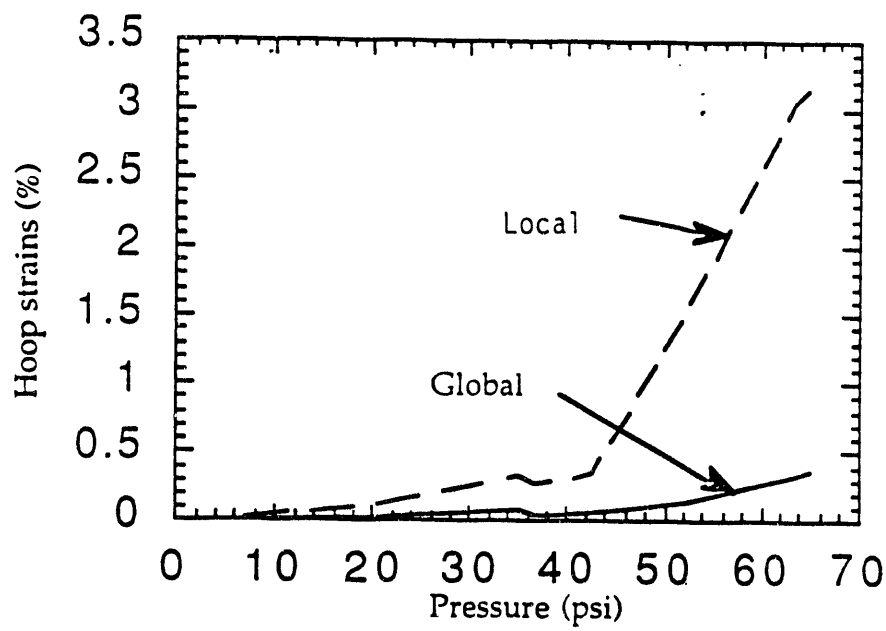

Figure 21 Strain at the Dome Steel Liner Discontinuity

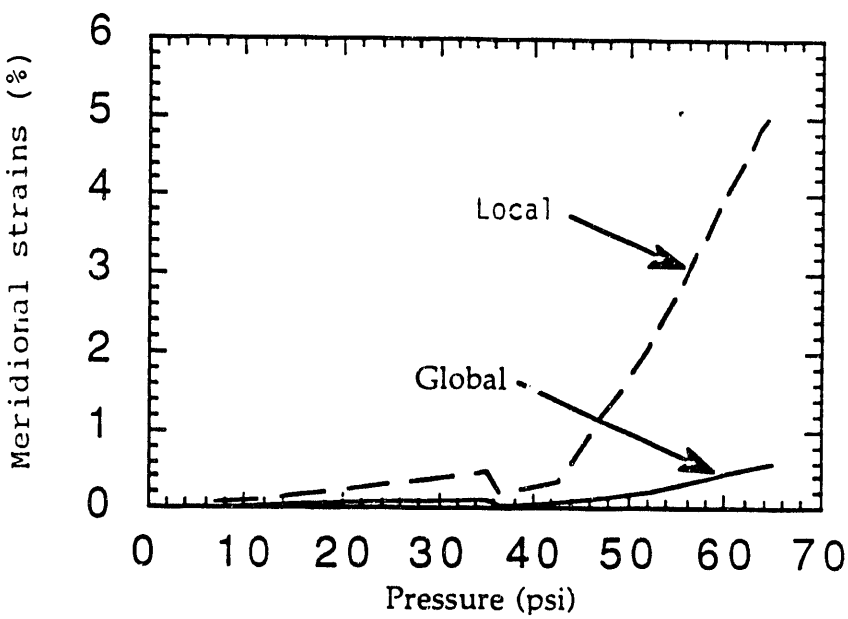

Figure 22 Strain Concentrations at the Dome Steel Liner Discontinuity

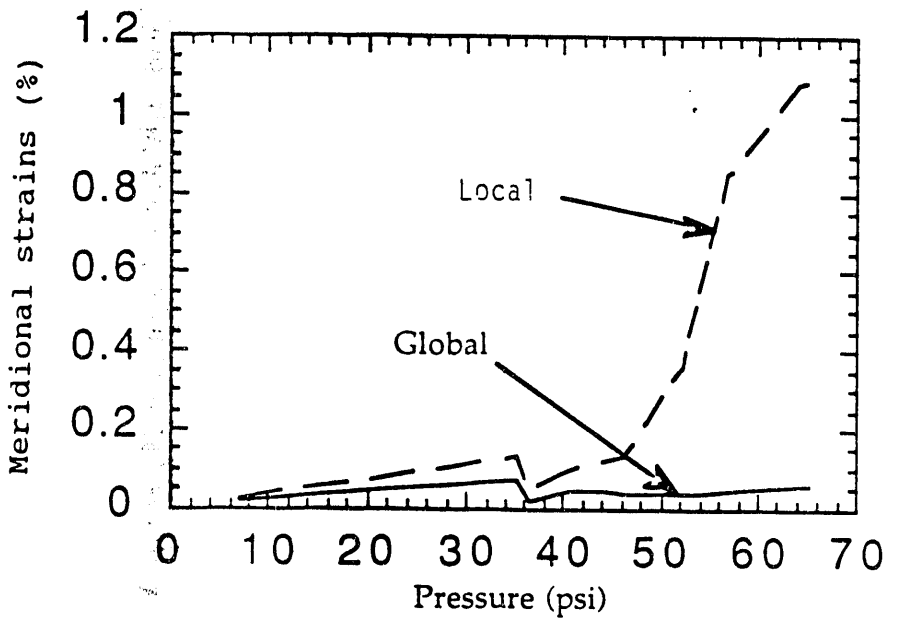

Figure 23 Strain concentrations at the base steel liner discontinuity

END

DATE
FILMED
5/28/93